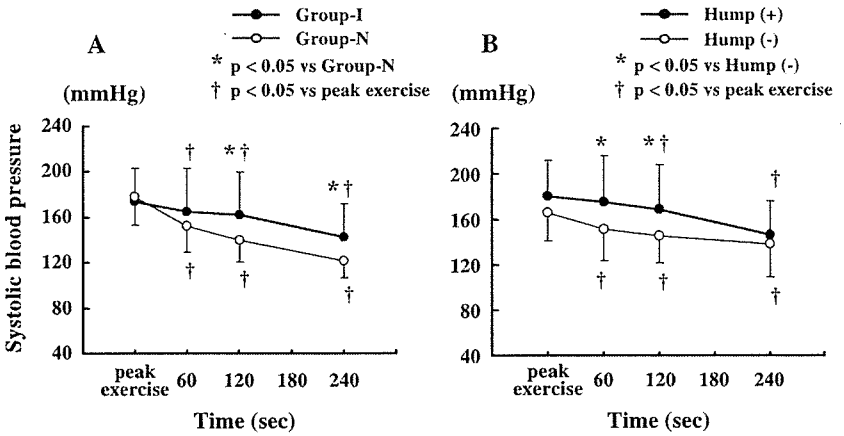

Fig. 5. Comparisons of systolic blood pressure time-course after exercise between Group-I and Group-N (A, left panel), and between the Group-I patients with and without "Hump" phenomenon (B, right panel).

may be electrically canceled by the opposite vector of ST elevation occurring in association with ventricular asynergy.

It is generally accepted that exercise-induced ST-segment elevation over post-infarct q-wave leads occurs in association with severe left ventricular asynergy, however, several studies indicated that exercise-induced ST-segment elevation might occur due to induced ischemia [21,22]. In the present study, we observed a similar prevalence of ST-segment elevation of ≥ 0.1 mV in Group-N (55%) and Group-I (47%, NS), suggesting that this index alone is of no use for identifying ischemia. We cannot exclude the possibility that ST-segment elevation might be caused by ischemia in some patients of Group-I, because three Group-I patients presented both exercise-induced ST-segment elevation and depression.

On the other hand, the present study has shown that abnormal transient VO_2 components after exercise, "Hump" phenomenon defined by our method described above, is a useful indicator for inducible ischemia in patients with acute anterior infarction. When the combination of $T_{max} \geq 40$ s and $D_{max} \geq 15\%$ were used for the definition of "Hump", we could diagnose inducible ischemia with sensitivity of 57%, specificity of 97%.

Abnormal postexercise VO_2 kinetics has been reported previously in patients with cardiocirculatory disorders. Hayasida et al. and other authors reported that the recovery of VO_2 was prolonged in patients with left ventricular dysfunction and that the time-course of VO_2 decay after exercise was closely related to exercise capacity [16–18,23–27] and prognosis [28]. Delayed energy store recovery in the skeletal muscle [22,24] and prolonged decrease in cardiac output [23,25–27,29] are considered to be involved in the genesis of this abnormal VO_2 recovery.

To our knowledge, there have been no published studies specifically examining the significance of exercise-induced ischemia on the postexercise abnormal VO_2 kinetics. Abnormal components of our interest, i.e., "Hump", is characterized by a transient convex bulge in the limited portion of VO_2 decay at around 1 min. The occurrence seems to appear not immediately but soon after the termination of exercise, generally lasting approximately 1 min. Previous reports estimated abnormal VO_2 kinetics by estimating the whole VO_2 decay with use of temporal parameters such as half time, [18,24,26] time constant [16,23,25] or cumulative area [28]. Since these measures are clearly unsuitable for our purpose, the non-exponential components (i.e., D-curve), that were derived by subtraction assuming that the abnormal components would be superimposed upon the monoexponential VO_2 decay, were compared between Group-I and Group-N. As a result, in Group-I, the mean value averaged over 30–60 s was greater than that averaged over 0–30 s, whereas such a difference was not found in Group-N (Fig. 2, upper two panels). Furthermore, the D-curve peaked later and its maximal value was greater in Group-I compared with Group-N (Fig. 2, lower two panels). Thus, the group difference of the D-curve with respect to the amplitude and temporal profile enabled us to identify the presence of inducible ischemia by the criterion shown in Table 3.

It was somewhat unexpected that some of patients without inducible ischemia (Group-N) showed a sizable amount of non-exponential components in the very early period of recovery up to 30 to 40 s. Our expectation was that non-exponential components in Group-N would be negligibly small, because the VO_2 decay curve should be closely fitted by the monoexponential model. This discrepancy indicates that postexercise VO_2 decay is not necessarily monoexponential in shape, and may be more precisely fitted by other mathematical models such as a sigmoidal model, even in the absence of inducible ischemia, although simple noise inherent in the measurements might be also related to the components. Impairment of LV function due to infarction and peripheral dysfunction caused by the immobilization (deconditioning effects) in the acute phase of myocardial infarction would contribute to the loss of the rapid fall of VO_2 immediately after exercise.

Several studies indicated that, in patients with inducible myocardial ischemia, an abnormal systolic blood pressure

response is observed not only during exercise but also during the recovery phase; a lesser decrease in systolic BP in the early recovery period, [10–15] which was in agreement with our results that the prolonged time-course of the postexercise decrease in systolic BP was seen in Group-I. It was also reported that, in these patients, stroke volume during exercise progressively decreased according to the development of severe ischemia, and it did not decrease but rather increased during the early period of recovery. [29–31] Although this paradoxical increase following exercise may occur either by a decrease in peripheral vascular tone after exercise [29,30] or by an improvement of LV function following the resolution of induced ischemia, [31] dynamic changes in the former factor are unlikely to transiently occur. The fact that, in Group-I, systolic BP at 1 min of recovery did not significantly decrease from peak exercise only in patients with "Hump", but not in patients without "Hump " reasonably suggests the direct role of enhanced stroke volume soon after exercise on the occurrence of "Hump".

The exact mechanism responsible for "Hump" is speculative, however, a recent study by Belardinelli et al. may provide a clue to the mechanism [32]. They indicated that exercise-induced ischemia resulting in a reduction in stroke volume decreases the increase rate of VO_2 to work rate increase (i.e., $\Delta VO_2/\Delta WR$) after the ischemic threshold. This reduction in $\Delta VO_2/\Delta WR$ would produce some amount of abnormal oxygen deficit (that is, extra-oxygen deficit), which might be paid back soon after exercise when the cardiac performance recovers. We consider that this process may be "Hump", transiently appearing on the limited portion of the early recovery of VO_2 decay. It should be noted that a reduction in $\Delta VO_2/\Delta WR$ during exercise was difficult to discern by visual inspection in any patient in our patients including those manifesting "Hump", probably because of a large spontaneous variations in VO_2 during exercise.

As described previously, it is possible that a mono-exponential curve used for deriving the non-exponential components is not be the most appropriate model for identifying "Hump". No single model may be suitable for fitting of the postexercise VO_2 decay, because the morphology of postexercise VO_2 decay curve considerably varied between individuals, probably due to the varying extent of impairment of LV function and the status of conditioning. Nevertheless, our method could identify "Hump" with a reasonable sensitivity and high specificity. Further investigation is necessary to ascertain this issue.

In conclusion, postexercise VO_2 "Hump" phenomenon, with its peak occurring around 60 s after exercise, seems to be a useful marker for inducible myocardial ischemia. The identification of this phenomenon may be more useful, particularly in patients with limited diagnostic accuracy of exercise ECG such as those with anterior myocardial infarction.

Acknowledgments

This study was supported by Research Grants for Cardiovascular Diseases (11C-7) from the Ministry of Health and Welfare of Japan, by Grant-in-Aid for Scientific Research (C-11670730) from the Japan Society for the Promotion of Science, and by the Program for Promotion of Fundamental Studies in Health Science from the Organization for Pharmaceutical Safety and Research.

References

[1] Taylor GJ, Humphries JO, Mellitis ED, et al. Predictors of clinical course, coronary anatomy and left ventricular function after recovery from acute myocardial infarction. Circulation 1980;62:960–70.
[2] Sanz G, Castoner A, Betriu A, et al. Determinants of prognosis in survivors of myocardial infarction: a prospective clinical angiographic study. N Engl J Med 1982;306:1065–70.
[3] De Feyter PJ, van Eeruge MJ, Dighton DH, et al. Prognostic value of exercise testing, coronary angiography and left ventriculography 6–8 weeks after myocardial infarction. Circulation 1982;66:527–36.
[4] Theruox P, Waters DD, Halpen C, et al. Prognostic value of exercise testing soon after myocardial infarction. N Engl J Med 1979;301: 341–5.
[5] Castellanet MJ, Greenberg PS, Ellestad MH. Comparison of ST-segment change on exercise testing with angiographic findings in patients with prior myocardial infarction. Am J Cardiol 1978;42: 29–35.
[6] Tilkemeier PL, Guiney TE, LaRaia PJ, et al. Prognostic value of predischarge low-level exercise thallium testing after thrombolytic treatment of acute myocardial infarction. Am J Cardiol 1990;66: 1203–7.
[7] Froelicher VF, Perdue ST, Atwood JE, et al. Exercise testing of patients recovering from myocardial infarction. Eur Probl Cardiol 1986;11:370–444.
[8] Haber HL, Beller GA, Watson DD, et al. Exercise thallium-201 scintigraphy after thrombolytic therapy with or without angiography for acute myocardial infarction. Am J Cardiol 1993;71:1257–61.
[9] Tomita T, Takaki H, Hara Y, et al. Attenuation of hypercapnic carbon dioxide chemosensitivity after postinfarction exercise training: possible contribution to the improvement in exercise hyperventilation. Heart 2003;9:404–10.
[10] Kato K, Saito F, Hatano K, et al. Prognostic value of abnormal postexercise systolic blood pressure response; prehospital discharge test after myocardial infarction in Japan. Am Heart J 1990;119: 264–71.
[11] Miyahara T, Yokota M, Iwase M, et al. Mechanism of abnormal postexercise systolic blood pressure response and its diagnostic value in patients with coronary artery disease. Am Heart J 1990;120:40–9.
[12] Tsuda M, Hatano K, Hayashi H, et al. Diagnostic value of postexercise systolic blood pressure response for detecting coronary artery disease in patients with or without hypertension. Am Heart J 1993;125:718–24.
[13] Abe K, Tsuda M, Hayashi H, et al. Diagnostic usefulness of postexercise systolic blood pressure response for detection of coronary artery disease in patients with electrocardiographic left ventricular hypertrophy. Am J Cardiol 1995;76:892–5.
[14] Hashimoto M, Okamoto M, Yamagata T, et al. Abnormal systolic blood pressure response during exercise recovery in patients with angina pectoris. J Am Coll Cardiol 1993;22:659–64.
[15] McHam SA, Marwick TH, Pashkow FJ, et al. Delayed systolic blood pressure recovery after graded exercise. J Am Coll Cardiol 1999; 34:754–9.

[16] Hayashida W, Kumada T, Kohno F, et al. Post-exercise oxygen uptake kinetics in patients with left ventricular dysfunction. Int J Cardiol 1993;38:63–72.
[17] Riley M, Stanford CF, Nicholls DP. Ventilatory and heart rate responses after exercise in chronic cardiac failure. Clin Sci (Lond) 1994;87:231–8.
[18] Cohen-Solal A, Laperche T, Morvan D, et al. Prolonged kinetics of recovery of oxygen consumption after maximal graded exercise in patients with chronic heart failure. Circulation 1995;91:2924–32.
[19] Hanley JA, McNeil BJ. A method of comparing the areas under receiver operating characteristic curves derived from the same cases. Radiology 1983;148:839–43.
[20] Manvi KM, Ellestd MH. Elevated ST segments with exercise in ventricular aneurysm. J Electrocardiol 1972;5:317–23.
[21] Miyakado H, Kato M, Noguchi N, et al. Exercise-induced ST-segment elevation-role of left ventricular wall motion abnormalities and coronary artery narrowing. Jpn Circ J 1995;59:725–35.
[22] Feyter PJ, Majid PA, Eenige MJ, Wardeh R, Wempe FN, Roos JP. Clinical significance of exercise-induced ST segment elevation. Correlative angiographic study in patients with ischemic heart disease. Br Heart J 1981;6:84–92.
[23] Kitaoka H, Takata J, Furuno T, et al. Delayed recovery of postexercise blood pressure in patients with chronic heart failure. Am J Cardiol 1997;79:1701–4.
[24] Cohen-Solal A, Czitrom D, Geneves M, et al. Delayed attainment of peak oxygen consumption after the end of exercise in patients with chronic heart failure. Int J Cardiol 1997;60:23–9.
[25] Pavia L, Myers J, Cesare R. Recovery kinetics of oxygen uptake and heart rate in patients with coronary artery disease and heart failure. Chest 1999;116:808–13.
[26] Tanabe Y, Takahashi M, Hosaka Y, et al. Prolonged recovery of cardiac output after maximal exercise in patients with chronic heart failure. J Am Coll Cardiol 2000;35:1228–36.
[27] Daida H, Allison TG, Johnson BD, et al. Further increase in oxygen uptake during early active recovery following maximal exercise in chronic heart failure. Chest 1996;109:47–51.
[28] Groote P, Millaire A, Decoulx E, et al. Kinetics of oxygen consumption during and after exercise in patients with dilated cardiomyopathy. New markers of exercise intolerance with clinical implications. J Am Coll Cardiol 1996;28:168–75.
[29] Koike A, Ito H, Doi M, et al. Beat-to-beat evaluation of cardiac function during recovery from upright bicycle exercise in patients with coronary artery disease. Am Heart J 1990;120:316–23.
[30] Plotnick GD, Becker LC, Fisher ML, et al. Changes in left ventricular function during recovery from upright bicycle exercise in normal persons and in patients with coronary artery disease. Am J Cardiol 1986;58:247–51.
[31] Schneider RM, Weintraub WS, Klein LW, et al. Rate of left ventricular functional recovery by radionuclide angiography after exercise in coronary artery disease. Am J Cardiol 1986;57:927–32.
[32] Belardinelli R, Lacalaprice F, Carle F, et al. Exercise-induced myocardial ischaemia detected by cardiopulmonary exercise testing. Eur Heart J 2003;24:1304–13.

J Pharmacol Sci 101, 214 – 222 (2006)

Journal of Pharmacological Sciences

Full Paper

Acetylcholine Inhibits the Hypoxia-Induced Reduction of Connexin43 Protein in Rat Cardiomyocytes

Yanan Zhang[1], Yoshihiko Kakinuma[2,*], Motonori Ando[2], Rajesh G Katare[2], Fumiyasu Yamasaki[1], Tetsuro Sugiura[1], and Takayuki Sato[2]

Departments of [1]Clinical Laboratory and [2]Cardiovascular Control, Kochi Medical School, Nankoku, Kochi 783-8505, Japan

Received December 14, 2005; Accepted May 8, 2006

Abstract. In a recent study, we demonstrated that vagal stimulation increases the survival of rats with myocardial infarction by inhibiting lethal arrhythmia through regulation of connexin43 (Cx43). However, the precise mechanisms for this effect remain to be elucidated. To investigate these mechanisms and the signal transduction for gap junction regulation, we investigated the effect of acetylcholine (ACh), a parasympathetic nerve system neurotransmitter, on the gap junction component Cx43 using H9c2 cells. When cells were subjected to hypoxia, the total Cx43 protein level was decreased. In contrast, pretreatment with ACh inhibited this effect. To investigate the signal transduction, cells were pretreated with L-NAME, a nitric oxide synthase inhibitor, followed by ACh and hypoxia. L-NAME was found to suppress the ACh effect. However, a NO donor, SNAP, partially inhibited the hypoxia-induced reduction in Cx43. To delineate the mechanisms of the decrease in Cx43 under hypoxia, cells were pretreated with MG132, a proteasome inhibitor. Proteasome inhibition produced a striking recovery of the decrease in the total Cx43 protein level under hypoxia. However, cotreatment with MG132 and ACh did not produce any further increase in the total Cx43 protein level. Functional studies using ACh or okadaic acid, a phosphatase inhibitor, revealed that both reagents inhibited the decrease in the dye transfer induced by hypoxia. These results suggest that ACh is responsible for restoring the decrease in the Cx43 protein level, resulting in functional activation of gap junctions.

Keywords: acetylcholine, connexin43, cardiomyocyte, hypoxia, proteasome inhibitor

Introduction

The prognosis of patients with chronic heart failure remains poor, despite the introduction of new pharmacological approaches and defibrillation devices, mainly due to lethal arrhythmia (1). Therefore, another therapeutic approach would be indispensable. In heart failure, the sympathetic nerve system is relatively activated compared with the parasympathetic nerve system (2), and this sympathetic nerve system-predominant condition is known to be involved in arrhythmogenicity. Recently, vagal nerve stimulation was reported to remarkably improve the survival rate of rats with heart failure due to myocardial infarction (3), suggesting that reactivation of the parasympathetic nerve system, which is suppressed in heart failure, plays a crucial role in attenuating the progression of heart failure. Moreover, our recent study revealed that acetylcholine (ACh), a parasympathetic nerve system neurotransmitter, plays an important role in regulating the protein level of the gap junction component connexin43 (Cx43) in the infarcted heart and cardiomyocytes under hypoxia (4). However, the precise mechanisms by which ACh regulates Cx43 remain to be elucidated. To investigate these mechanisms, we focused on Cx43 in H9c2 cells.

Gap junctions are intercellular junctions, and several connexin family members, including Cx43, participate in their formation. Among the connexin family members, Cx43 is the principal electrical coupling

*Corresponding author. kakinuma@med.kochi-u.ac.jp
Published online in J-STAGE: July 7, 2006
doi: 10.1254/jphs.FP0051023

protein in ventricles, while Cx40 plays the same role in atria. The functions of Cx43 are regulated by phosphorylation as well as the protein level. Cx43 phosphorylation can modulate the channel properties and turnover dynamics. SDS-PAGE of Cx43 generally reveals a faster non-phosphorylated isoform (NP-Cx43) and slower phosphorylated isoforms (P-Cx43). Cx43 is synthesized in the rough endoplasmic reticulum, transported to the Golgi apparatus, and ultimately trafficked to the plasma membrane (5, 6). Recent evidence has suggested that Cx43 is involved in modifying arrhythmogenic conditions (7, 8) since Cx43 knockout mice were subject to sudden death caused by lethal arrhythmia, including ventricular tachycardia, or fibrillation (9, 10). Although many other factors, including sodium, potassium, and calcium channels, appear to be involved in arrhythmogenicity, it is speculated that functional deletion of Cx43 is also responsible for arrhythmia. To date, it has remained unclear whether and how ACh modulates Cx43. Therefore, we focused on the effect of ACh on Cx43.

Materials and Methods

Cell culture and pharmacological agents

H9c2 cells, which are spontaneously immortalized ventricular myoblasts from rat embryos, were used due to their conserved electrical and signal transduction characteristics (11). The cells were cultured in DMEM supplemented with 10% FBS and antibiotics. H9c2 cells were pretreated with 1 mM ACh for 8 h, followed by 1 h of hypoxia (1% of oxygen concentration). We chose N^{ω}-nitro-L-arginine methyl ester (L-NAME) (Sigma Chemical Co., St Louis, MO, USA), a specific nitric oxide (NO) synthase inhibitor, to determine whether NO mediates the signal transduction for Cx43 expression. L-NAME (1 mM) was administered for 1 h together with ACh, followed by hypoxia for 1 h. H9c2 cells were also treated with 1 mM *S*-nitroso-*N*-acetyl-l,l-penicillamine (SNAP) (Sigma Chemical Co.) before hypoxia. We used 10 μM Cbz-leu-leu-leucinal (MG132) (Sigma Chemical Co.) or 1 μM okadaic acid to investigate whether hypoxia enhanced Cx43 degradation or phosphorylation was important for regulating the functional activity of Cx43.

Western blot analysis

Cells were harvested from the dishes and prepared for immunoblotting as described previously (8). After washing in PBS, cells were lysed with SDS sample buffer and boiled for 10 min. After electrophoresis in a 10% SDS-polyacrylamide gel, proteins were transferred to a polyvinylidene difluoride membrane. The membrane was soaked in 4% skim milk in TBST solution overnight, then incubated with an anti-Cx43 polyclonal antibody (ZYMED Laboratories, Inc., South San Francisco, CA, USA) for 1 h, thoroughly washed, and then incubated with an anti-rabbit IgG secondary antibody (BD Transduction Laboratories, San Diego, CA, USA) for 40 min. Finally, the membrane was washed and subjected to chemiluminescent detection using the ECL Plus Western Blotting Detection Reagents (Amersham Biosciences, Piscataway, NJ, USA). We performed repeatedly 3-5 times each experiment using duplicate samples. The Western blotting data were analyzed using Kodak 1D Image Analysis Software (Eastman Kodak Co., Rochester, NY, USA).

Immunohistochemistry

H9c2 cells were fixed with 4% paraformaldehyde for 10 min and permeabilized with 1% Triton X-100 for another 10 min. To block nonspecific antibody binding, cells were incubated with 5% skim milk and successively incubated with an anti-Cx43 polyclonal antibody (ZYMED Laboratories, Inc.), in 1% skim milk at 4°C overnight and then with a Cy3-labeled secondary antibody (Jackson ImmunoReserch Laboratories, West Grove, PA, USA) at 4°C overnight. Actin staining was performed using FITC-conjugated phalloidin and then examined with a laser scanning confocal microscope.

Functional analysis of gap junction using a scrape and scratch method

A scrape-loading method can be used to introduce macromolecules into cultured cells by inducing a transient tear in the plasma membrane without affecting cell viability, thereby allowing sensitive determination of cell-cell communication. Following the treatment with ACh or okadaic acid, cells cultured on a coverslip were rinsed with PBS, and then 1% Lucifer Yellow was applied to the center of the converslip. A 27 gauge needle was used to create two longitudinal scratches through the cell monolayer. The cells were incubated in the dye mix for exactly 1 min, quickly rinsed three times with PBS, and finally examined by fluorescence microscopy. Lucifer Yellow does not diffuse through intact plasma membranes, but its low molecular weight permits its transmission from one cell to another, presumably across patent gap junctions (12 – 16). The area of the dye transferred from the scratched margin in hypoxia or hypoxia with ACh treatment was semi-quantified using the NIH image system and compared with that in normoxia.

Statistical analyses

Data are presented as the mean ± S.E.M. Differences

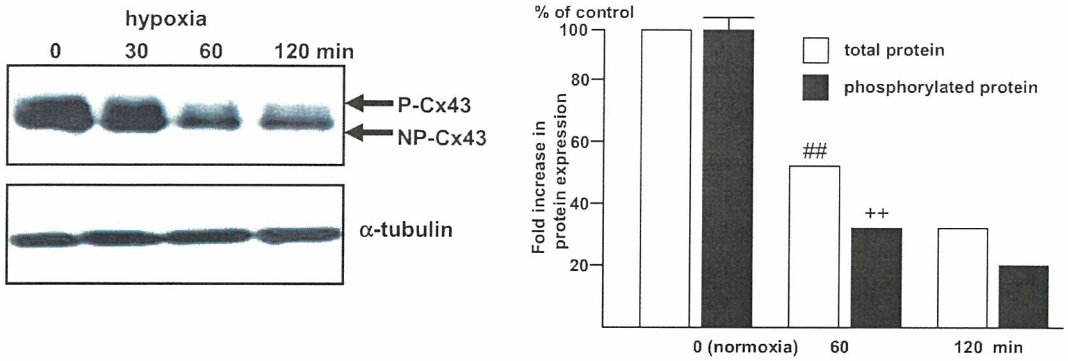

Fig. 1. Cx43 phosphorylation is decreased by hypoxia. Cells are subjected to 30 – 120 min of hypoxia and then analyzed by Western blot analysis. Cx43 phosphorylation (P-Cx43) is reduced to 32 ± 4% of the level under normoxia ($^{++}P<0.01$ *vs* 0 min, $^{\#\#}P<0.01$ *vs* 0 min) by 1% hypoxia, and the effect is remarkable after 60 min of hypoxia. NP-Cx43: non-phosphorylated form of Cx43. Open bars: total Cx43 protein level, closed bars: P-Cx43 level. Representative data from 5 independently performed experiments are shown (n = 5).

were assessed by ANOVA followed by Fisher's PLSD for multiple comparisons. The results were considered statistically significant at the level of $P<0.05$.

Results

Hypoxia decreases the Cx43 protein level in H9c2 cells

Several different forms of Cx43 were observed in the case of H9c2 cell (Fig. 1). The upper bands represented the phosphorylated forms, while the lower band corresponded to the non-phosphorylated form. We examined the acute effect of hypoxia on the total Cx43 protein level in H9c2 cells (n = 5). The total protein level of Cx43, including NP-Cx43 and P-Cx43, gradually decreased during hypoxia (Fig. 1), and 60 min of hypoxia induced a remarkable decrease in the total Cx43 protein level ($^{\#\#}P<0.01$ *vs* 0 min of hypoxia) and reduced its phosphorylation to 32 ± 4% of the normoxic level ($^{++}P<0.01$ *vs* 0 min of hypoxia). These results suggest that the total Cx43 protein level is rapidly decreased under hypoxia.

ACh increases the Cx43 protein level in H9c2 cells under normoxia or hypoxia

To determine whether ACh could modulate the Cx43 protein level after acute treatment, we initially treated H9c2 cells with 1 mM ACh under normoxia (n = 3). When the cells were stimulated with 1 mM ACh under normoxia, the Cx43 protein level was transiently increased ($^{++}P<0.01$ *vs* 0 min), followed by a rapid decrease, and then another peak was observed at 8 h (Fig. 2A). Next, to examine the effect of ACh on the hypoxia-induced decrease in Cx43, we pretreated H9c2 cells with 1 mM of ACh for 7 h, followed by 1 h of hypoxia (n = 6). Compared to the Cx43 level under hypoxia alone (hypoxia), the Cx43 protein level in ACh-pretreated H9c2 cells was not decreased under hypoxia (ACh + hypoxia), but instead was rather sustained ($^{\#\#}P<0.01$ *vs* hypoxia; ns, not significant *vs* normoxia; n = 6) (Fig. 2B). This ACh-mediated inhibition of the decrease in Cx43 under hypoxia was also observed by immunocytochemistry since hypoxia decreased the Cx43 immunoreactivity, and ACh inhibited the reduction (Fig. 2C).

Inhibition of the decrease in the Cx43 protein level during hypoxia by ACh occurs via NO

To further characterize the signal transduction for ACh-mediated inhibition of the reduction in the Cx43 protein level under hypoxia, we investigated the effects of chemicals on the Cx43 protein level (n = 5) (Fig. 3). Pretreatment with L-NAME (1 mM) for 1 h inhibited the ACh-induced recovery of the Cx43 protein level during hypoxia, suggesting that NO participates in regulating the Cx43 protein level ($^{\#}P<0.05$ *vs* ACh, n = 5). To further investigate whether the protein level was affected by NO, the cells were treated with 1 mM SNAP, a NO donor, instead of ACh. SNAP partially inhibited the reduction in the Cx43 protein level compared with L-NAME treatment, further suggesting that NO plays a partial role in modulating the protein level ($^{+}P<0.05$ *vs* L-NAME, n = 5).

Cx43 is degraded under hypoxia

To further investigate the mechanisms of the decrease in Cx43 under hypoxia, H9c2 cells were pretreated with the proteasome inhibitor MG132 (n = 5) for 10 and 60 min during hypoxia (Fig. 4A). The proteasome inhibition produced a striking recovery of the decreased total Cx43 protein level. MG132 inhibited the reduction

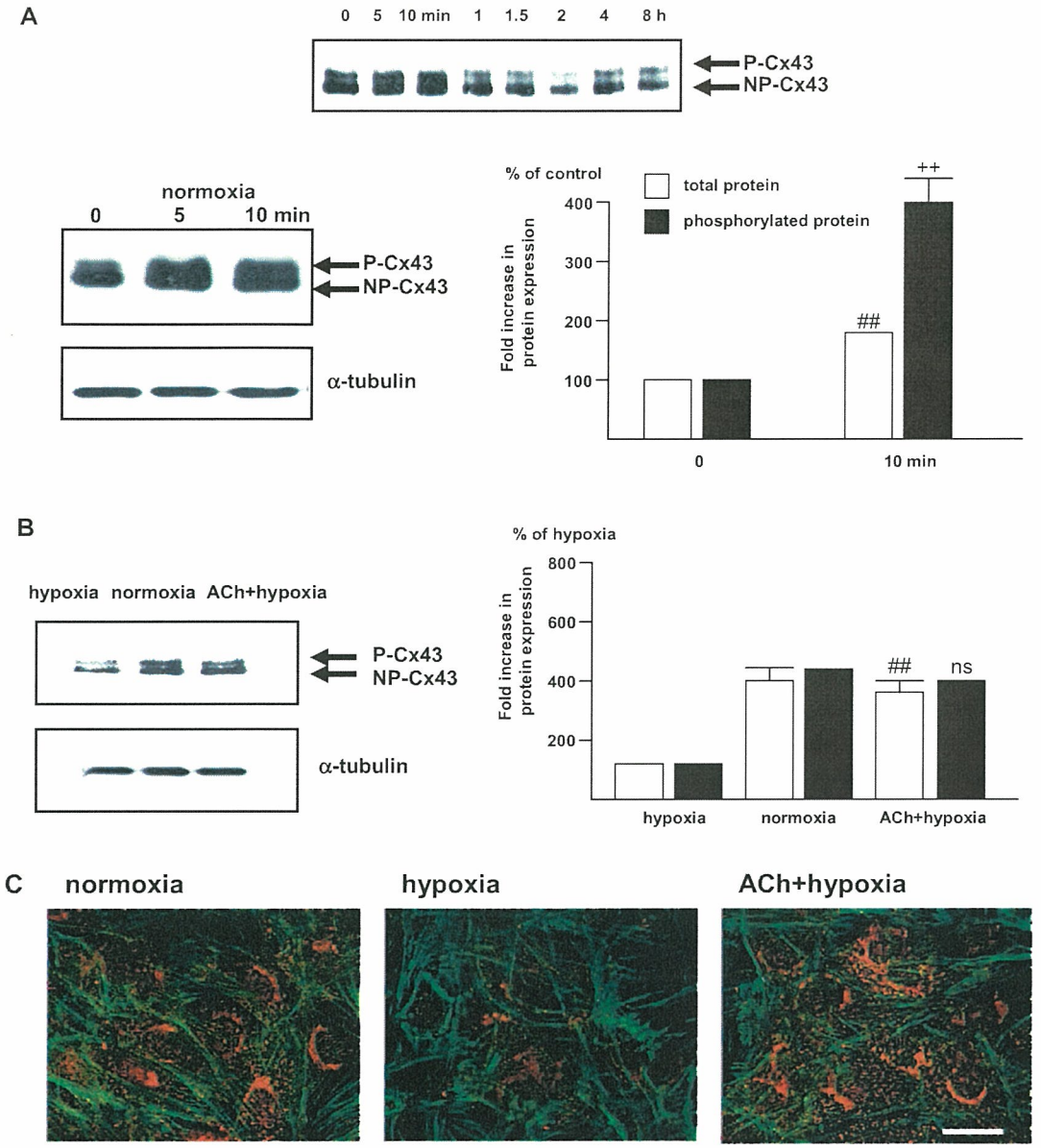

Fig. 2. ACh regulates Cx43 phosphorylation under normoxia and hypoxia. A: 1 mM ACh increases Cx43 phosphorylation (P-Cx43) in the acute phase under normoxia, reaching a peak of 409 ± 28% at 10 min ($^{++}P<0.01$ *vs* 0 min, $^{\#\#}P<0.01$ *vs* 0 min, n = 3). The entire time course shows another peak of the Cx43 protein level following the acute phase at 8 h. B: ACh suppresses the reduction in the Cx43 protein level induced by 1 h of hypoxia. ACh (1 mM) pretreated H9c2 cells show a sustained level of Cx43 phosphorylation, comparable to that under normoxia (normoxia), even under hypoxia (ACh + hypoxia) ($^{\#\#}P<0.01$ *vs* hypoxia; ns, not significant *vs* normoxia; n = 6). C: ACh inhibits the reduction in Cx43 immunoreactivity under hypoxia (red dots). Representative staining is shown. Cx43 is indicated by red dots. Bar: 50 μm.

in the Cx43 protein level by hypoxia for up to 60 min, suggesting that the reduction is due to activation of Cx43 protein degradation ($^{\#}P<0.05$ *vs* normoxia, n = 5). Furthermore, the effect of MG132 on inhibiting Cx43 degradation was not modified by ACh addition, and as a consequence, the effect of MG132 on inhibiting the hypoxia-induced decrease in Cx43 was comparable to that of cotreatment with MG132 and ACh (not significant *vs* ACh + MG132, n = 5) (Fig. 4B). These results suggest that ACh modulates the degradation process of Cx43.

ACh activates the function of gap junctions through an increase in the Cx43 protein level

To investigate whether ACh inhibition of the Cx43 protein level during hypoxia leads to functional recovery of gap junctions, we applied the scrape/scratch technique (n = 5). In a control experiment, scrape-loaded

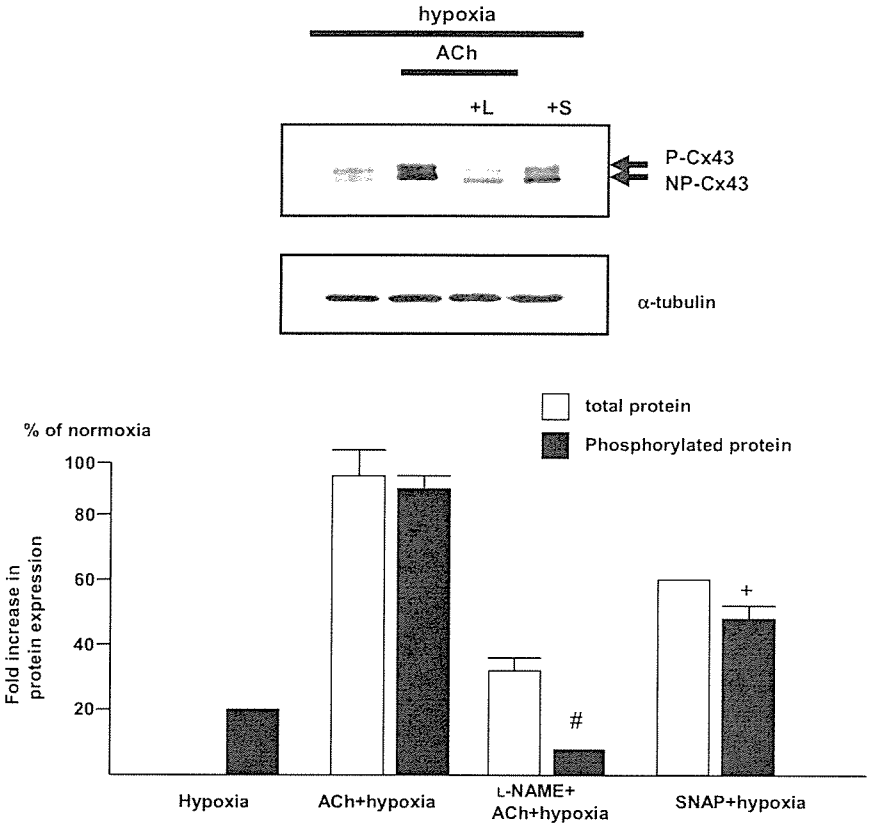

Fig. 3. NO is involved in the ACh signaling pathway that leads to the increase in Cx43 phosphorylation ($^{\#}P<0.05$ *vs* ACh + hypoxia; $^{+}P<0.05$ *vs* L-NAME + ACh + hypoxia). ACh: 1 mM ACh, L: 1 mM L-NAME, S: 1 mM SNAP. Representative data from 5 independently performed experiments are shown (n = 5).

cells in the presence of Lucifer Yellow showed positive transfer of Lucifer Yellow between cells. In contrast, cells treated with hypoxia appeared to lose their ability to communicate with each other and the dye transfer was blocked to 6 ± 2% of the intensity under normoxia. In contrast, ACh suppressed the hypoxia-induced blockage of dye transfer ($^{\#\#}P<0.01$ *vs* hypoxia, not significant *vs* normoxia, n = 5). The area of Lucifer Yellow fluorescence was increased in ACh-treated cells along the scraped margin during hypoxia (62 ± 10% of the area under normoxia) (Fig. 5). These results suggest that hypoxia affects intercellular communication and that ACh functionally activates cell-cell communication, even under hypoxia, through increases in the Cx43 protein level. Furthermore, pretreatment with 1 μM okadaic acid, a phosphatase inhibitor, for 10 min recovered the reduction in the Cx43 protein level and the extent of dye transfer during hypoxia (Fig. 6). Taken together with the results obtained with the proteasome and phosphatase inhibitors, it is suggested that both the protein and phosphorylation levels of Cx43 are involved in the function of Cx43.

Discussion

In the current study, we have shown that the Cx43 protein level is regulated by ACh in the presence or absence of hypoxia. Even in normoxia, ACh regulated the Cx43 protein level and inhibited the reduction in the Cx43 protein level induced under hypoxia. Such modification of the Cx43 protein level by ACh partially occurred via NO, since the protein level sustained by ACh during hypoxia was affected by L-NAME, whereas SNAP showed similar effects to ACh. Furthermore, the results indicated that the hypoxia-induced decrease in the total Cx43 protein level is due to proteasome degradation. Taken together, these results further suggest that ACh is involved in inhibiting Cx43 degradation under hypoxia.

Our previous study revealed that vagal stimulation inhibited the reduction in the Cx43 protein level during acute myocardial ischemia and instead sustained a similar level to that in the normal heart (4). As a result, vagal stimulation was further shown to decrease the frequency of ventricular arrhythmia. Moreover, ACh sustained the dye transfer level, which was attenuated

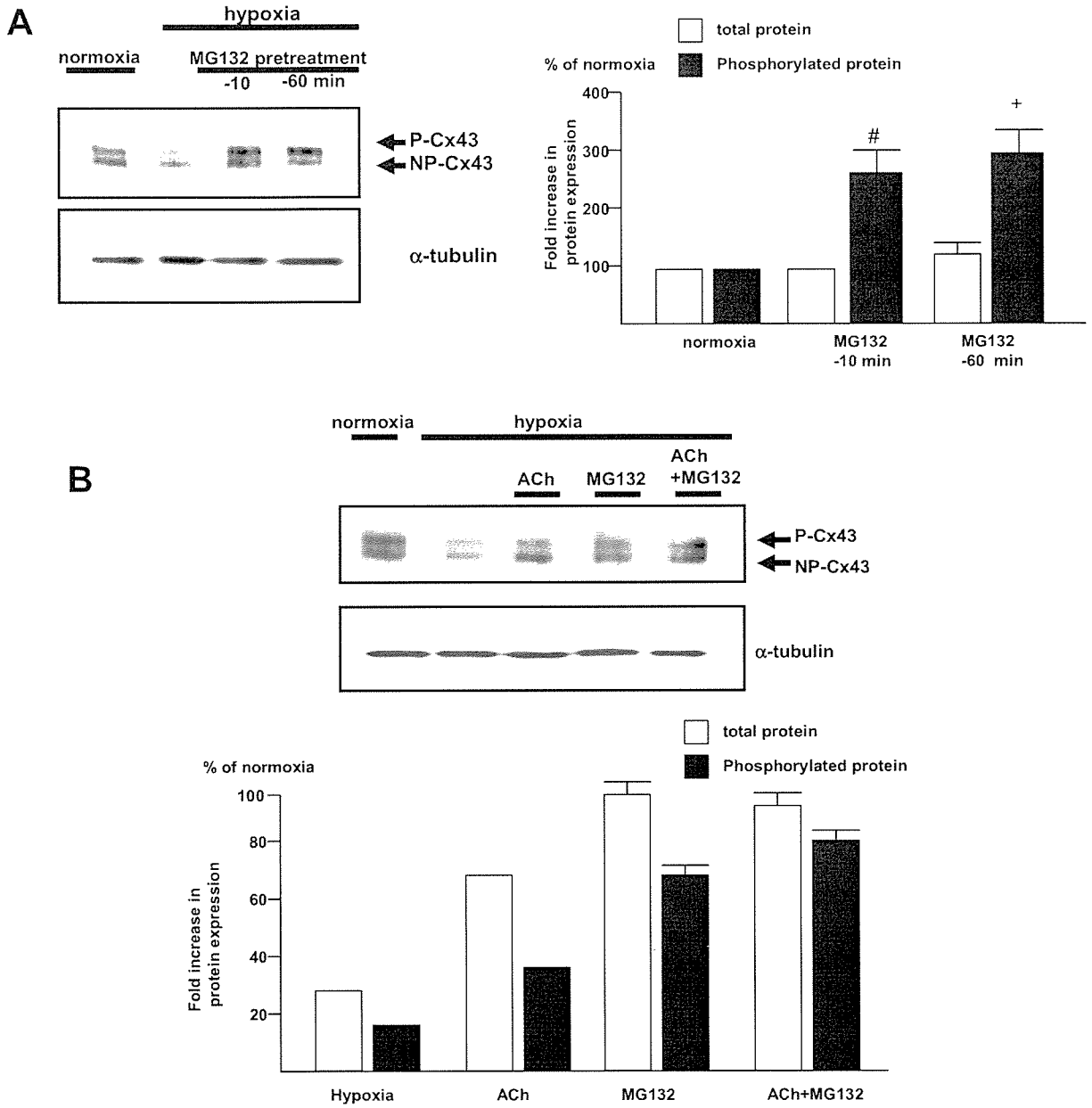

Fig. 4. MG132, a proteasome inhibitor, increases the Cx43 protein level during hypoxia, and cotreatment with ACh does not change this effect. A: Pretreatment with MG132 inhibits the reduction in Cx43 phosphorylation induced by hypoxia ($^{\#}P<0.05$ *vs* normoxia; $^{+}P<0.05$ *vs* normoxia, n = 5). Normoxia: no MG132 or hypoxia. The cells were pretreated with 10 μmol/L MG132 before and at 10 and 60 min of hypoxia. B: The effect of MG132 on inhibiting the reduction in Cx43 phosphorylation is not accentuated by cotreatment with 1 mM ACh since the level of Cx43 phosphorylation with ACh + MG132 is comparable to that with MG132 alone (not significant *vs* MG132, n = 5). Representative data from 5 independently performed experiments are shown (n = 5).

under hypoxia, to the same level observed under normoxia. On the basis of the finding that the survival of Cx43 knockout mice was extremely poor due to ventricular arrhythmia (9, 10), it is suggested that ACh regulates Cx43, which may inhibit arrhythmia.

Our immunohistochemical study supported the result that ACh greatly suppressed the reduction in the Cx43 level under hypoxia. L-NAME inhibited the effect of ACh on Cx43, whereas SNAP mimicked the ACh effect, suggesting that NO is involved in the signaling pathway. ACh is able to induce NO production (17) and has a cardioprotective effect both in vivo and in vitro (18, 19). In fact, H9c2 cells were reported to generate NO from mitochondria in response to ACh (20). Taken together,

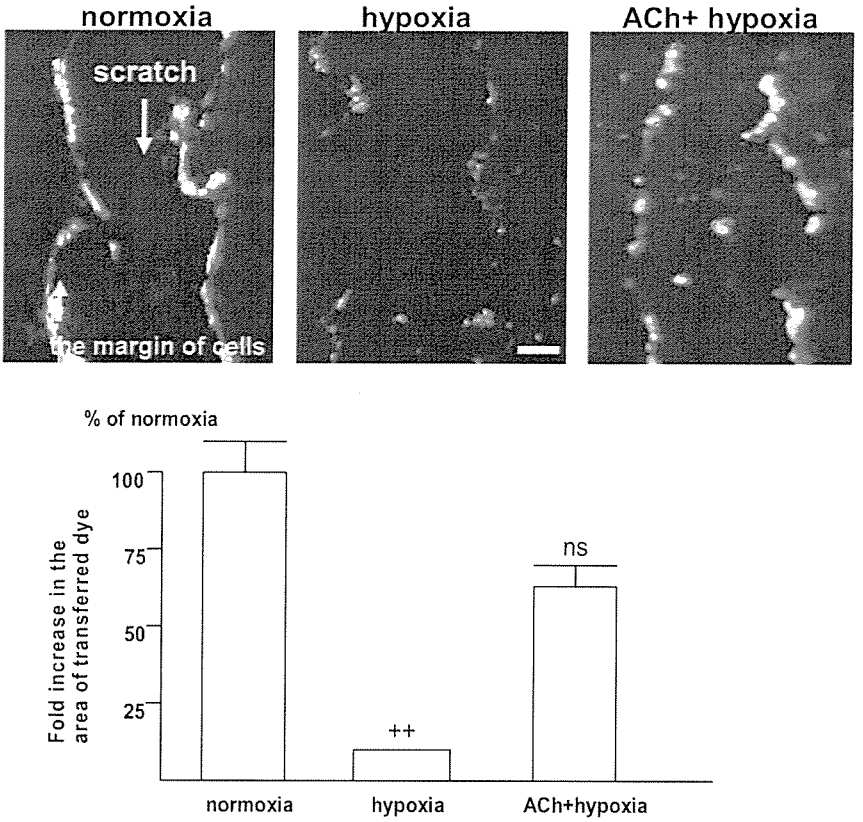

Fig. 5. Fluorescence photomicrographs of scrape/scratch experiments using Lucifer Yellow. Intercellular communication is blocked in H9c2 cells treated with 60 min of hypoxia (hypoxia) ($^{++}P<0.01$ *vs* hypoxia, n = 5). ACh (1 mM) reverses the blockage of intercellular communication induced by hypoxia (ACh + hypoxia) to a comparable level to the control (ns, not significant *vs* normoxia; n = 5) Bar: 150 μm.

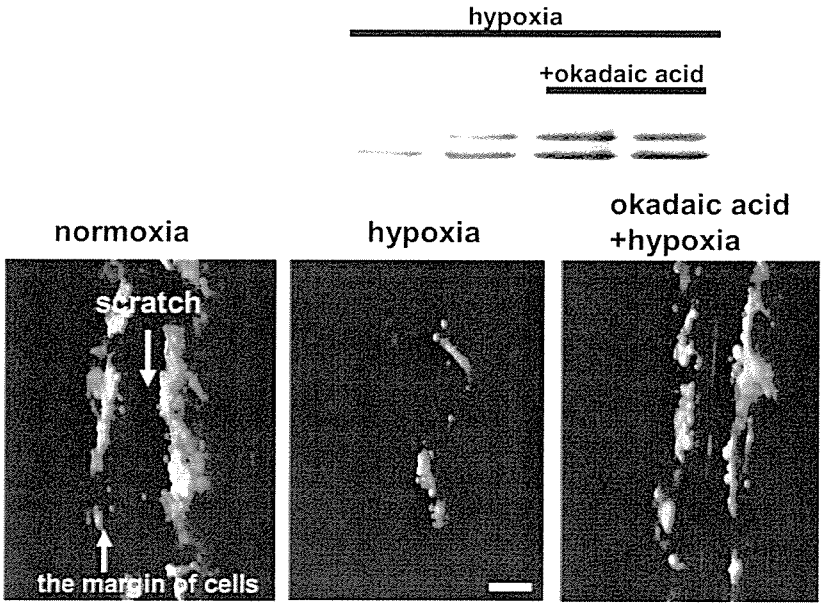

Fig. 6. Phosphatase inhibition recovers cell-cell communication during hypoxia. Pretreatment with okadaic acid (1 μm) for 10 min before hypoxia inhibits the reduction in the Cx43 protein level during hypoxia. Furthermore, it reverses the dye transfer blockage under hypoxia, similar to ACh. Representative data from 3 independently performed experiments are shown (n = 3). Bar: 150 μm.

it is suggested that ACh regulates the Cx43 protein level in cardiomyocytes partly through NO.

To explore whether the Cx43 level during hypoxia was regulated by proteasome degradation, we treated cells with the proteasome inhibitor MG132. Recently, several types of low-molecular-weight proteasome inhibitors have been developed that can readily enter cells and selectively inhibit the protein-degradation pathway. Although their toxicities may sometimes be troublesome experimentally, cell viability and growth are not generally affected by short treatments with these molecules (21 – 23). Surprisingly, MG132 increased the Cx43 protein level, which was reduced under hypoxia, to a comparable level to that after ACh treatment. However, the effect of MG132 on the recovery of Cx43 was not affected by cotreatment with ACh. These results suggest that the proteasome pathway plays a role in Cx43 degradation and that ACh modulates the degradation of Cx43 during hypoxia.

The results of the present study have demonstrated that the increased Cx43 protein level contributes to the functional improvement of gap junctions under hypoxia using the scrape/scratch method. The ACh-induced increase in the Cx43 protein level was functionally involved in the cell-cell communication since ACh recovered Lucifer Yellow transport from the margin of the scratched regions, even under in hypoxia.

As well as the total protein level, the Cx43 phosphorylation level was shown to be involved in its function. Specifically, okadaic acid, a phosphatase inhibitor, recovered the Cx43 protein level and the extent of dye transfer under hypoxia, suggesting that dephosphorylation was partially involved in the hypoxia-induced degradation, eventually leading to a decrease in the total Cx43 protein level. To date, several phosphorylation sites of Cx43 have been reported to have positive or negative effects on gap junctions, suggesting that their function depends on these phosphorylation sites (24). Although we did not investigate the specific phosphorylation site regulated by ACh in the present study, our results suggest that ACh modulates the function of gap junctions through both the protein and phosphorylation levels of Cx43.

Although the scrape/scratch method has some limitations for evaluating cell-cell communication, the result obtained were compatible with those in our previous dye injection study under chemical hypoxia, that is, ACh-treated cardiomyocytes efficiently transferred the dye to surrounding cells, even under hypoxia (4). Therefore, these results suggest that inhibition of the decrease in the Cx43 protein level by ACh under hypoxia is responsible for the enhanced cell-cell communication.

H9c2 cells have been shown to retain several characteristics of the electrical and hormonal signaling pathways found in adult cardiomyocytes and are therefore a useful model for cardiomyocytes from the aspect of signal transduction. The cells show similar morphological characteristics to immature embryonic cardiomyocytes (20).

In conclusion, the results of the present study suggest that ACh activates cell-cell communication by sustaining the Cx43 protein level during hypoxia through modification of the Cx43 degradation pathway.

Acknowledgment

This study was supported by a Health and Labor Sciences Research Grant (H15-PHYSI-001) for Advanced Medical Technology from Ministry of Health, Labor, and Welfare of Japan.

References

1 Janse MJ. Electrophysiological changes in heart failure and their relationship to arrhythmogenesis. Cardiovasc Res. 2004;61:208–217.
2 Prado MAM, Reis RAM, Prado VF, de Mello MC, Gomez MV, de Mello PG. Regulation of acetylcholine synthesis and storage. Neurochem Int. 2002;41:291–299.
3 Li M, Zheng C, Sato T, Kawada T, Sugimachi M, Sunagawa K. Vagal nerve stimulation markedly improves long-term survival after chronic heart failure in rats. Circulation. 2004;109:120–124.
4 Ando M, Katare GR, Kakinuma Y, Zhang D, Yamasaki F, Muramoto K, et al. Efferent vagal nerve stimulation protects heart against ischemia-induced arrhythmias by preserving connexin43 protein. Circulation. 2005;12:164–170.
5 Musil LS, Goodenough DA. Biochemical analysis of connexin43 intracellular transport, phosphorylation, and assembly into gap junctional plaques. J Cell Biol. 1991;115:1357–1374.
6 Lamp PD, Lau AF. Regulation of gap junctions by phosphorylation of connexins. Arch Biochem Biophys. 2000;384:205–215.
7 Moon C-H, Jung Y-S, Kim MH, Park RM, Lee SH, Baik EJ. Protein kinase C inhibitors attenuate protective effect of high glucose against hypoxic injury in H9c2 cardiac cells. Jpn J Physiol. 2000;50:645–649.
8 Jain SK, Schuessler RB, Saffitz JE. Mechanisms of delayed electrical uncoupling induced by ischemic preconditioning. Circ Res. 2003;92:1138–1144.
9 van Rijen HV, Eckardt D, Degen J, Theis M, Ott T, Willecke K, et al. Slow conduction and enhanced anisotropy increase the propensity for ventricular tachyarrhythmias in adult mice with induced deletion of connexin43. Circulation. 2004;109:1048–1055.
10 Gutstein DE, Morley GE, Vaidya D, Liu F, Chen FL, Stuhlmann H, et al. Conduction slowing and sudden arrhythmic death in mice with cardiac-restricted inactivation of connexin43. Circ Res. 2001;88:333–339.

11 Hescheler J, Meyer R, Plant S, Krautwurst D, Rosenthal W, Rosenthal W, et al. Morphological, biochemical, and electrophysiological characterization of a clonal cell (H9c2) line from rat heart. Circ Res. 1991;69:1476–1486.
12 Le A-CN, Musil LS. Normal differentiation of cultured lens cells after inhibition of gap junction-mediated intercellular communication. Dev Biol. 1998;204:80–96.
13 Musil LS, Le A-CN, Vanslyke JK, Roberts LM. Regulation of connexin degradation as a mechanism to increase gap junction assembly and function. J Biol Chem. 2000;275:25207–25215.
14 McNeil PL, Murphy RF, Lanni F, Taylor DL. A method for incorporating macromolecules into adherent cells. J Cell Biol. 1984;98:1556–1564.
15 El-Fouly MH, Trosko JE, Chang C-C. Scrape-loading and dye transfer. A rapid and simple technique to study gap junctional intercellular communication. Exp Cell Res. 1987;168:422–430.
16 Stewart WW. Functional connections between cells as revealed by dye-coupling with a highly fluorescent naphthalimide tracer. Cell. 1978;14:741–759.
17 Liu H, Mcpherson BC, Zhu X, Da Costa MA, Jeevanandam V, Yao Z. Role of nitric oxide and protein kinase C in ACh-induced cardioprotection. Am J Physiol Heart Circ Physiol. 2001;281: H191–H197.
18 Rakhit R, Edwards RJ, Mockridge JW, Baydoun AR, Wyatt AW, Mann GE, et al. Nitric oxide, nitrates and ischaemic preconditioning. Am J Physiol Heart Circ Physiol. 2000;278: H1211–H1217.
19 Monastyrskaya E, Folarin N, Malyshev I, Green C, Andreeva L. Application of the nitric oxide donor SNAP to cardiomyocytes in culture provides protection against oxidative stress. Nitric Oxide. 2002;7:127–131.
20 Zanella B, Calonghi N, Pagnotta E, Masotti L, Guarnieri C. Mitochondrial nitric oxide localization in H9c2 cells revealed by confocal microscopy. Biochem Biophys Res Commun. 2002;290:1010–1014.
21 Lee DH, Goldberg AL. Proteasome inhibitors: valuable new tools for cell biologists. Trends Cell Biol. 1998;8:397–403.
22 Laing JG, Beyer EC. The gap junction protein connexin43 is degraded via the ubiquitin proteasome pathway. J Biol Chem. 1995;270:26399–26403.
23 Lampe PD, Tenbroek EM, Brut JM, Kurata WE, Johnson RG, Lau AF. Phosphorylation of connexin43 on serine368 by protein kinase C regulates gap junctional communication. J Cell Biol. 2000;149:1503–1512.
24 Lampe PD, Lau AF. The effects of connexin phosphorylation on gap junctional communication. Int J Biochem Cell Biol. 2004;36:1171–1186.

Functional Neuroscience: Evoked Potentials and Related Techniques
(Supplements to Clinical Neurophysiology, Vol. 59)
Editors: C. Barber, S. Tsuji, S. Tobimatsu, T. Uozumi, N. Akamatsu, A. Eisen

Chapter 35

Partial conduction block in cervical compression myelopathies: waveform changes of ascending spinal evoked potentials

Toshikazu Tani*, Takahiro Ushida, Shinichirou Taniguchi, Kenji Ishida, Hideshi Tsuboya and Tatsunori Ikemoto

Department of Orthopedics, Kochi Medical School, Kohasu Oko-cho, Nankoku City, Kochi 783-8505 (Japan)

1. Introduction

Conduction block is probably the most important, potentially treatable cause for clinical weakness and sensory loss in compression myelopathies (Kimura and Kaji, 1991; Waxman et al., 1995). Multisegmental recording of ascending spinal evoked potentials (EPs) from the structures adjacent to the spinal cord after epidural stimulation helps to precisely localize the site of conduction block for surgical intervention in the presence of multilevel compression (Tani et al., 1995). In this case, an abrupt reduction in size of the negative wave over a short segment is taken as a strong evidence for a focal conduction block (McDonald and Sears, 1970; Cornblath et al., 1991). In particular, monophasic positive EPs immediately rostral to compression characterizes a complete focal conduction block as an easily recognizable waveform change (Woodbury, 1965; Deecke and Tator, 1973; Schramm et al., 1983), since a blocked fiber gives rise to a killed-end effect producing only a volume-conducted positive wave rostral to conduction block (Woodbury, 1965; Tani et al., 1997).

Partial, as compared to complete conduction block, is common in chronic compression myelopathies, the recognition of conduction block becomes more difficult with increasing number of unblocked fibers. This is partly because physiologic temporal dispersion also reduces the EP size with increasing distance between stimulating and pickup electrodes, mimicking partial conduction block (Olney and Miller, 1984; Cornblath et al., 1991; Kimura and Kaji, 1991). In our previous report (Tani et al., 1997), a computer simulation predicted that preferential blocks of fast-conducting fibers increase the initial positive peak of the EP at the site of conduction block, even if the negative peak reduction is small. An enhancement of the negative peak immediately caudal to conduction block, as also predicted by the computer model (Tani et al., 1997) and actually observed with complete conduction block (Tani et al., 1998), may serve to differentiate partial conduction block from physiologic temporal dispersion. Applying these principles to identify partial conduction block, we looked at the correlation between the site of partial conduction block and MRI abnormalities in cervical compression myelopathies.

Correspondence to: Toshikazu Tani, M.D., Department of Orthopedics, Kochi Medical School, Kohasu Oko-cho, Nankoku City, Kochi 783-8505, Japan.
Tel: 81-88-880-2385; Fax: 81-88-880-2388;
E-mail: tanit@med.kochi-u.ac.jp

2. Materials and methods

2.1. Patients

From July 1991 to July 2001, 65 patients with compression myelopathies underwent multisegmental EP studies during posterior decompression surgeries for moderate to severe spastic limb paresis. Informed consent was obtained. Of these, 24 patients showed a complete focal conduction block and 5 others, gradual or complicated waveform changes. We analyzed the recordings in the remaining 36 patients with focal waveform changes consistent with partial conduction block. Myelopathy resulted from cervical spondylosis (21), ossified posterior longitudinal ligament (OPLL) (10), rheumatoid arthritis of the cervical spine (2), and extramedullary tumor (3). There were 23 men and 13 women ranging in age from 24 to 84 years (average age, 59 years). Based on the functional grading of Nurick (1972), 2 patients walked normally despite signs of spinal cord compromise (grade 1), 22 had some difficulty, but were able to ambulate unaided (grade 2), 9 required walking aids (grades 3 and 4), and 3 were chairbound or bedridden (grade 5). Twenty-five patients (69%) had lost fine finger movement in doing up buttons and opening and closing the fists (Crandall and Batzdorf, 1966; Ono et al., 1987). All but 6 showed sensory impairment for light touch, pinprick, or vibration in the upper limb and all but 5 in the lower limb. Of the 21 patients with bladder symptoms, 20 had hesitancy and urgency and, one retention and incontinence. Stretch reflexes were generally hyperactive although responses were diminished for the biceps in 6 patients, in the triceps in 2, in the gastrocnemius in 4. Extensor plantar responses were elicited in 14 patients.

2.2. Electrodiagnosis

All recordings were made in the operating rooms of Kochi Medical School after preoperative general anesthesia. A pair of stimulating electrodes (UKG-100-2PM, Unique Medical Corp, Tokyo, Japan), with two platinum tips at the end of an 18-gauge polyethylene tube, were introduced into the dorsal epidural space at the lumbar or lower thoracic level via a Tuohy needle

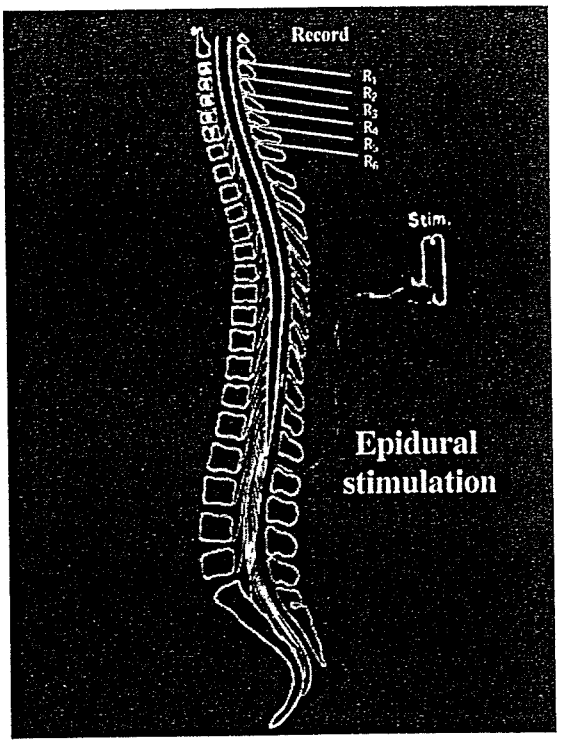

Fig. 1. Schematic drawing of the electrodiagnostic technique during posterior surgery. A pair of stimulating electrodes, with two platinum tips at the end of an 18-gauge polyethylene tube, were introduced into the dorsal epidural space at the lumbar or lower thoracic level via a Tuohy needle. Needle electrodes (G1) were inserted into the ligamentum flavum in the midline at serial intervertebral spaces. A series of needle electrodes (G2) inserted into the paraspinal muscles at the same level as G1 served as the reference.

(Shimoji et al., 1971; Tamaki et al., 1981) (Fig. 1). Electrical stimulation consisted of a square wave, 0.1 ms in duration and 20–40 mA in intensity, delivered at a rate of 3–20/s.

After exposure of the posterior aspect of the vertebrae, the needle electrodes (G1) (Dantec 13R23) were inserted into the ligamentum flavum in the midline at serial intervertebral spaces (Satomi et al., 1988; Matsuda and Shimazu, 1989; Pelosi et al., 1991; Tani et al., 1998) (Fig. 1). A series of needle electrodes (G2) (Dantec 13R21) inserted into the erector spinae muscles at the same level as G1 served as the reference. A pair of alligator clips was attached to the skin at the operative site as ground electrodes. The recordings were obtained simultaneously from 4 to 7 serial vertebral

levels between the occiput and T2 spine, according to the extent of vertebral exposure required for the respective decompression surgeries. Each test set comprised an average of 50–200 summated potentials with a frequency response of 20–5 kHz. An 8-channel averager (Dantec Evomatic 8000) allowed simultaneous recording of EPs from all sets of electrodes. Two tracings obtained for each electrode derivation confirmed consistency.

Measurements of EPs included:

(1) latencies from the stimulus artifact to the initial positive peaks;
(2) amplitudes from the baseline to the initial positive and the major negative peaks; and
(3) areas under the initial positive and the negative phases (see Figs. 2 and 3).

As shown in Figs. 2 and 3, 0 represented the site of conduction block identified by abrupt waveform changes, with other levels numbered in the order of increasing distance from the 0 level, assigning a minus sign caudally.

2.3. MRI evaluation

All patients underwent surface coil MR examination of cervical spinal cord preoperatively with one of the three superconducting systems (0.5 T MRT-50 and 1.5 T MRT-200; Toshiba Corp, Tokyo, Japan, 1.5 T Signa; GE Corp, Milwaukee, USA). The MRI protocol included sagittal and axial T1-weighted images, and sagittal T2-weighted images, with a slice thickness of 5 mm. The spin echo pulse sequences were 300–600 ms/9–30 ms (TR ms/TE ms) for T1 and 1500–4700 ms/40–117 ms for T2-weighted images.

Cord measurements at each intervertebral level from C2–3 to C6–7 included:

(1) anteroposterior diameter by a vernier caliper to the nearest 0.1 mm on midsagittal T1-weighted images, and
(2) cross-sectional area on axial T1-weighted images using a digitizer (Mitablet-II KD 4030 A; Graphtec Corp., Yokohama, Japan). The values were converted to the actual diameter and area using appropriate magnification factors. Attention was also directed, on sagittal T2-weighted images, to increased signal intensity resulting from cord compression (Takahashi et al., 1989).

2.4. Statistical analysis

The one-way analysis of variance (ANOVA) followed by Fisher's PLSD test was used to determine whether significant differences existed between values reported in the tables. The Wilcoxon signed rank test was used when comparing the negative peak amplitude and area between "0" level and "+1" or "+2" level in the patients who had EP recordings up to "+2" level. Values are given as mean ± SD and were considered significant at a probability (p) value of < 0.05.

3. Results

3.1. EPs

Incremental EP studies in 36 patients uncovered a single site of partial conduction block designated as "0", 3 each at C1–2 and C2–3, 9 at C3–4, 11 at C4–5, 9 at C5–6, and 1 at C6–7. At this level, the amplitude and area of the negative component were reduced (both $p < 0.0001$) to 43 ± 21% (range, 0–85%) and 37 ± 23% (range, 0–92%), respectively, compared to the "–1" level, which was taken as the baseline (100%) (Table 1 and Figs. 2 and 3). The negative component that was reduced to 0% at "0" level reappeared at the rostral levels, thus indicating a partial, not a complete, conduction block. In contrast, the initial positive component was increased ($p < 0.0001$) to 174 ± 95% (range, 67–495%) in amplitude and 403 ± 531% (72–2693%) in area (Table 2 and Figs. 2 and 3). In addition, the latency increase was greater from "–1" to "0" (0.60 ± 0.36 ms) than from "–2" to "–1" (0.34 ± 0.13 ms; $p < 0.0001$) and from "0" to "+1" (0.42 ± 0.29 ms; $p = 0.0018$).

Caudal to the site of conduction block, the negative component tended to increase in size progressively from "–4" to "–1," showing significant changes from "–3" to "–2" ($p = 0.011$) and from "–2" to "–1" ($p = 0.0135$) for area, but did not significantly increase in amplitude (Table 1 and Figs. 2 and 3).

Rostral to the site of conduction block, the negative component showed no significant change in size

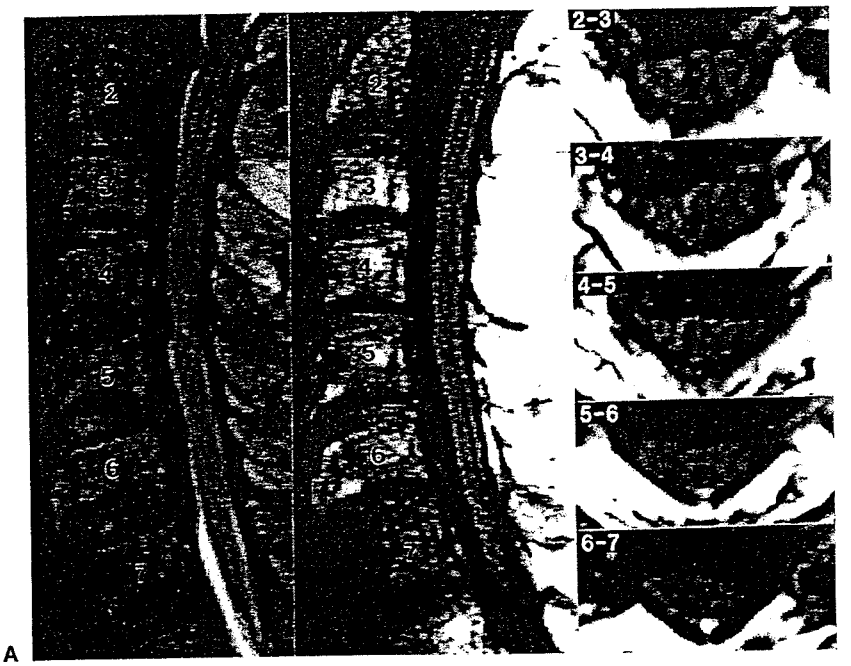

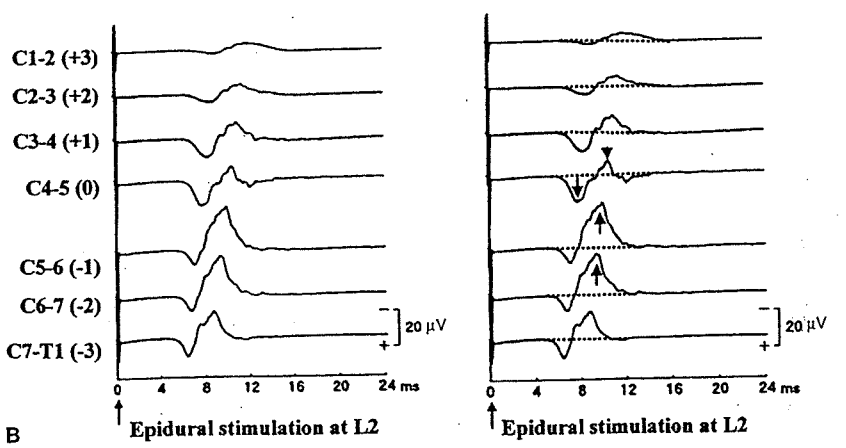

Fig. 2. (A) A sagittal T2-weighted MRI (TR 4411 ms; TE 92 ms) (left), and sagittal (middle), and axial (right) T1-weighted MRIs (TR 450 ms; TE 12 ms) in a 57-year-old man with cervical OPLL. Cord compression at C4–5 is greatest in terms of cross-sectional area, and equivalent to those at C2–3, C3–4, and C5–6 in terms of anteroposterior diameter. A deformed cord is seen at C2–3 through C6–7. An intramedullary high signal on T2-weighted image is seen at C4–5. (B) Recording of EPs obtained from the same patient as in (A). The EPs were recorded unipolarly from the ligamentum flavum of C7–T1 through C1–2 after epidural stimulation at L2. The numerical label for each recording site is indicated on the left side. Drawing the baselines with dotted lines (right) helps identify conduction block. The negative peak progressively increases in size from C7–T1 (–3) to C5–6 (–1) (arrows pointing up). This is followed by an abrupt reduction of the negative peak (arrow head) with concomitant augmentation of the initial positive peak (arrow pointing down) and the last positive peak at C4–5 (0). Note that the negative component is larger at C3–4 (+1) than at C4–5 (0).

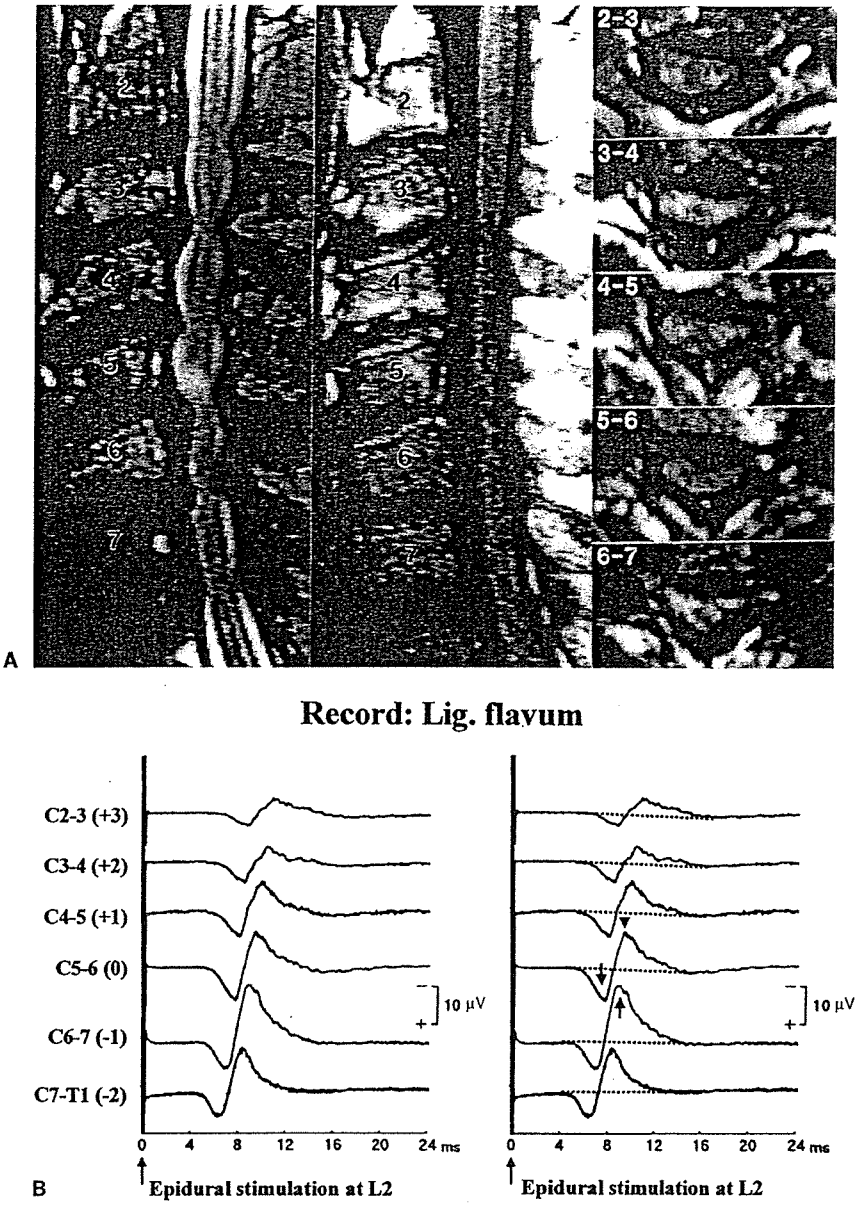

Fig. 3. (A) A sagittal T2-weighted MRI (TR 3636 ms; TE 96 ms) (left), and sagittal (middle), and axial (right) T1-weighted MRIs (TR 350 ms; TE 24 ms) in a 62-year-old man with cervical spondylotic myelopathy. Both the anteroposterior diameter and the cross-sectional area of the cord are smallest at C5–6, whereas a deformed cord is seen at C2–3 through C6–7. A high-intensity cord signal on T2-weighted image is also seen at C5–6. (B) Recording of EPs obtained from the same patient as in (A). The EPs were recorded unipolarly from the ligamentum flavum of C7–T1 through C2–3 after epidural stimulation at L2. The numerical label for each recording site is indicated on the left side. Drawing the baselines with dotted lines (right) helps identify conduction block. Note the increase in size of the negative peak (arrow pointing up) from C7–T1 (–2) to C6–7 (–1) followed by a reduction of the peak (arrow head) with a concomitant augmentation of the initial positive peak (arrow pointing down) at C5–6 (0).

TABLE 1

NEGATIVE PEAK OF EP

Recording level	Number of patients	Amplitude			Area		
		Mean (range) (μV)	Mean ± SD (%)	*p* value	Mean (range) (μV × ms)	Mean ± SD (%)	*p* value
+3	12	6.5 (0.7–29.5)	32 ± 15	NS	14.3 (0.3–55.2)	37 ± 22	NS
+2	27	5.4 (0.3–45.5)	31 ± 20	NS	11.0 (0.4–81.4)	32 ± 26	NS
+1	36	6.1 (0.4–33.0)	39 ± 24	NS	12.0 (0.1–50.7)	39 ± 32	NS
0	36	6.6 (0–42.9)	43 ± 21	<0.0001	11.3 (0–52.8)	37 ± 23	<0.0001
−1	36	16.4 (1.5–86.6)	100	NS	33.6 (3.9–120.0)	100	0.0135
−2	36	15.6 (1.3–86.6)	94 ± 17	NS	28.3 (3.4–110.6)	87 ± 19	0.011
−3	24	15.4 (0.9–73.2)	87 ± 20	NS	23.9 (1.7–88.4)	72 ± 21	NS
−4	11	12.4 (0.6–25.1)	84 ± 21		20.3 (1.1–40.5)	61 ± 22	

p values were based on the one-way analysis of variance followed by Fisher's PLSD test.

between two adjacent levels, in contrast to the initial positive component with a significant reduction in amplitude and area from "0" to "+1" and from "+1" to "+2" (Tables 1 and 2). In 27 patients who had EP recordings up to "+2" level, the negative component at "+1" or "+2" was significantly greater in area (42 ± 34% vs. 33 ± 24%; $p = 0.0198$), but not in amplitude, than at "0" (Fig. 2).

3.2. MRI

In the 36 patients with partial conduction block at single levels, sagittal and axial T1-weighted MRIs disclosed cord indentation at 78 levels and a deformed cord at 134 levels, respectively. Table 3 summarizes quantitative assessment of the cord compression in relation to the level of conduction block ("0" level). The "0" level always had both cord indentation and a deformed cord, showing a significantly smaller anteroposterior diameter ($p \leq 0.0002$) and cross-sectional area ($p \leq 0.0261$) of the cord compared to the remaining more caudal or rostral levels. However, the anteroposterior diameter or cross-sectional area of the cord was equally reduced or smaller at more caudal levels in 7 patients, at more rostral levels in 2, and at both more caudal and rostral levels in 4. Sagittal T2-weighted images disclosed high-intensity spinal cord signals at 27 levels in 22 patients. All matched the site of conduction block with the exception of five levels; two each located at "−1" and "−2" and one at "+1."

4. Discussion

Electrophysiological documentation of conduction block in chronic compression myelopathies plays an important role in elucidating the site responsible for the main functional change, particularly in the patients who have MRI evidence of multilevel compression (Tani et al., 1995). A conduction block in a single axon can be clearly identified by recording the action potential evoked in the nerve fiber. However, assessment of a spinal tract as a whole usually reveals more complicated features, because of the existence of interaction between potentials from constituent nerve fibers of different diameters. A major reduction in size of the compound sensory potential can result from physiologic desynchronization of the axonal volleys (Buchthal and Rosenfalck, 1966; Dorfman, 1984; Kimura et al., 1988). Thus, the evaluation of partial conduction block, as opposed to complete block, in the spinal cord, based on analysis of compound action potentials, requires careful exclusion of physiologic temporal dispersion that could substantially alter the waveform.

TABLE 2

POSITIVE PEAK OF EP

Recording level	Number of patients	Amplitude			Area			Latency		
		Mean (range) (μV)	Mean ± SD (%)	*p* value	Mean (range) (μV × ms)	Mean ± SD (%)	*p* value	Mean ± SD (ms)	Difference (ms)	*p* value
+3	12	4.1 (0.5–20.5)	47 ± 20	NS	4.2 (0.7–23.6)	73 ± 55	NS	6.78 ± 1.97	0.35 ± 0.11	
+2	27	3.8 (0.2–31.3)	73 ± 41	0.0018	5.1 (0.1–34.8)	122 ± 110	0.0301	7.08 ± 2.11	0.31 ± 0.14	NS
+1	36	5.7 (0.1–41.1)	122 ± 90	0.0004	8.8 (0.3–51.2)	264 ± 266	0.0214	6.81 ± 2.00	0.42 ± 0.29	NS
0	36	8.7 (0.5–45.1)	174 ± 95	<0.0001	16.2 (0.7–114.0)	403 ± 531	< 0.0001	6.39 ± 1.97	0.60 ± 0.36	0.0018
−1	36	6.1 (0.2–41.1)	100	NS	5.4 (0.1–34.0)	100	NS	5.79 ± 1.74	0.34 ± 0.13	< 0.0001
−2	36	6.6 (0.3–45.5)	110 ± 28	NS	5.4 (0.4–31.3)	118 ± 63	NS	5.45 ± 1.69	0.41 ± 0.16	NS
−3	24	7.7 (0.6–50.0)	131 ± 59	NS	6.6 (0.7–32.3)	155 ± 165	NS	5.22 ± 1.63	0.27 ± 0.09	NS
−4	11	6.3 (0.4–15.7)	151 ± 51		6.5 (0.6–21.0)	191 ± 151		4.65 ± 1.90		

p values were based on the one-way analysis of variance followed by Fisher's PLSD test.

TABLE 3

CERVICAL CORD MEASUREMENT

Intervertebral level	Number of patients	Anteroposterior diameter		Cross-sectional area	
		Mean ± SD	Range (mm)	Mean ± SD	Range (mm^2)
+3	10	6.2 ± 1.8	3.1–9.7	68.5 ± 19.9	41.7–99.2
+2	20	6.1 ± 1.5	3.8–9.5	70.7 ± 17.8	43.9–103.5
+1	30	5.7 ± 1.4	2.6–8.5	70.0 ± 17.3	25.9–95.5
0	36	4.0 ± 1.1*	1.7–6.2	51.2 ± 14.0*	17.3–77.6
–1	35	5.7 ± 1.0	3.8–7.8	64.8 ± 14.8	35.5–102.6
–2	26	5.9 ± 1.2	2.8–7.6	66.9 ± 13.3	39.9–92.7
–3	15	6.0 ± 0.7	4.8–7.2	64.4 ± 16.5	34.8–89.6

*Significantly smaller anteroposterior diameter ($p \leq 0.0002$) and cross-sectional area ($p \leq 0.0261$) of the cord than those at the remaining more caudal and rostral levels. p values were based on the one-way analysis of variance followed by Fisher's PLSD test.

The present study has shown that recording of ascending EPs in short increments helps identify a partial conduction block to localize a focal lesion. In surface recording at multiple levels for peripheral compressive neuropathies, the amplitude of nerve action potentials is greatly affected by the depth of the nerve from the skin surface. In contrast, intraoperative multisegmental recording registers comparable EPs, because all recording electrodes are nearly equidistant to the spinal cord if placed in the structures adjacent to the spinal cord such as ligamentum flavum. This technique can be carried out during surgery before decompression procedures.

We measured the positive and negative components of the EP separately to delineate the characteristic waveform changes of each component, which are affected differently. In this series of patients, the negative peak was significantly diminished at the site of conduction block compared to the immediately caudal level, although the degree of diminution ranged widely among different patients from a subtle (15%) to an extreme (100%) reduction in amplitude. With a subtle reduction of the negative peak, the presence of a concomitant enlargement of the initial positive peak or the incremental change of negative peaks caudal to that level, or both, distinguished partial conduction block from physiologic temporal dispersion. Without conduction block at the "0" level, the negative peak would have been progressively smaller in size from "–4" to "–1," as predicted from physiologic temporal dispersion. With an extreme reduction of the negative peak, its reappearance rostrally supported the diagnosis of partial, not complete, conduction block. The phenomenon of partial recovery of the negative peak beyond the site of conduction block was, although counter-intuitive, by no means the exception but the rule in partial conduction block. In fact, the area of the negative component was significantly greater either at "+1" or "+2" than at "0" in the patients who had EP recordings up to "+2" level.

A model using solid angle approximation (Woodbury, 1965; Brown, 1968; Tani et al., 1997; Kimura, 2001) and the concept of phase cancellation (Kimura et al., 1988; Kimura, 1998) can provide possible mechanisms that account for the above-mentioned waveform changes near the site of partial conduction block. The EP can be conceived of as a linear summation of potentials arising from constituent nerve fibers (Stegeman et al., 1979). If peaks of opposite polarity overlap, the EP will diminish in size because of phase cancellation (Kimura, 1988). At the site of conduction block, a blocked fiber contributes a normal